Békési *et al. Geothermal Energy* (2022) 10:3
https://doi.org/10.1186/s40517-022-00214-6

Geothermal Energy

RESEARCH Open Access

Ground motions induced by pore pressure changes at the Szentes geothermal area, SE Hungary

Eszter Békési[1,2*], Peter A. Fokker[1,3], Thibault Candela[3], János Szanyi[4] and Jan-Diederik van Wees[1,3]

*Correspondence:
bekesi.eszti23@gmail.com
[1] Utrecht University, 3584 CB Utrecht, Netherlands
Full list of author information is available at the end of the article

Abstract

Excessive thermal water volumes have been extracted from porous sedimentary rocks in the Hungarian part of the Pannonian Basin. Thermal water production in Hungary increased significantly from the early 1970s. Regional-scale exploitation of geothermal reservoirs without re-injection resulted in basin-scale pressure drop in the Upper Pannonian (Upper Miocene) sediments, leading to compaction. This compaction resulted in ground subsidence primarily through poro-elastic coupling.

We investigated surface deformation at the Szentes geothermal filed, SE Hungary, where the largest pressure decline occurred. Subsequently, hydraulic head recovery in the western part of the geothermal reservoir was initiated in the mid-1990s. We obtained data from the European Space Agency's Envisat satellites to estimate the ground motions for the period of November 2002–December 2006. We applied inverse geomechanical modeling to estimate reservoir properties and processes. We constrained the model parameters using the Ensemble Smoother with Multiple Data Assimilation, which allowed us to incorporate large amounts of surface movement observations in a computationally efficient way. Ground movements together with the modeling results show that uplift of the Szentes geothermal field occurred during the observation period. Since no injection wells were operated at Szentes before 2018, and production temperatures remained relatively constant through the entire production period, we explain ground uplift with pore pressure increase due to natural recharge. The estimated decompaction coefficients of the reservoir system characterizing the elastic behavior of the Szentes geothermal reservoir varies between ~ 0.2×10^{-9} and 2×10^{-9} Pa^{-1}. Compaction coefficients of the reservoir system corresponding to the earlier depressurization period, from ~ 1970 to the mid-1990s, may be significantly larger due to the potential inelastic behavior and permanent compaction of clay-rich aquitards. The improved parametrization enables better forecasting of the reservoir behavior and facilitates the assessment of future subsidence scenarios that are helpful for the establishment of a sustainable production scheme.

Keywords: InSAR, Geomechanical modeling, Data assimilation, Szentes geothermal field (Hungary)

Introduction

Hungary is among the most favorable countries for geothermal development within Europe (e.g., Békési et al. 2018; Cloetingh et al. 2010; Horváth et al. 2015; Lenkey et al. 2021; Limberger et al. 2014, 2018), with an average geothermal gradient of ~ 45 °C/km, and a mean surface heat flow of 100 mW/m^2 (Lenkey et al. 2002). The highest values occur in the SE part of the country, corresponding to the thinnest parts of the crust and lithosphere (e.g., Horváth et al. 2006). The outstanding geothermal conditions of Hungary originate from Miocene extension of the Pannonian Basin, related to subduction and roll-back in the Eastern Carpathians, resulting in the thermal attenuation of the lithosphere (e.g., Horváth 1993; Horváth et al. 2006). The different timing of syn-rift sediment infill in the sub-basins indicates that extension in the Pannonian Basin migrated in space and time (e.g., Fig. 1b) (Balázs et al. 2016). Subsequent to the syn-rift phase, thermal subsidence of the Pannonian Basin initiated, accompanied by continuous post-rift sedimentation (e.g., Juhász 1991; Sztanó et al. 2013). From Late Miocene to recent times, basin inversion has occurred due to a push from the Adriatic microplate towards the Pannonian Basin (Bada et al. 2007; Horváth and Cloetingh 1996), forming its present-day basement geometry (Fig. 1a, b).

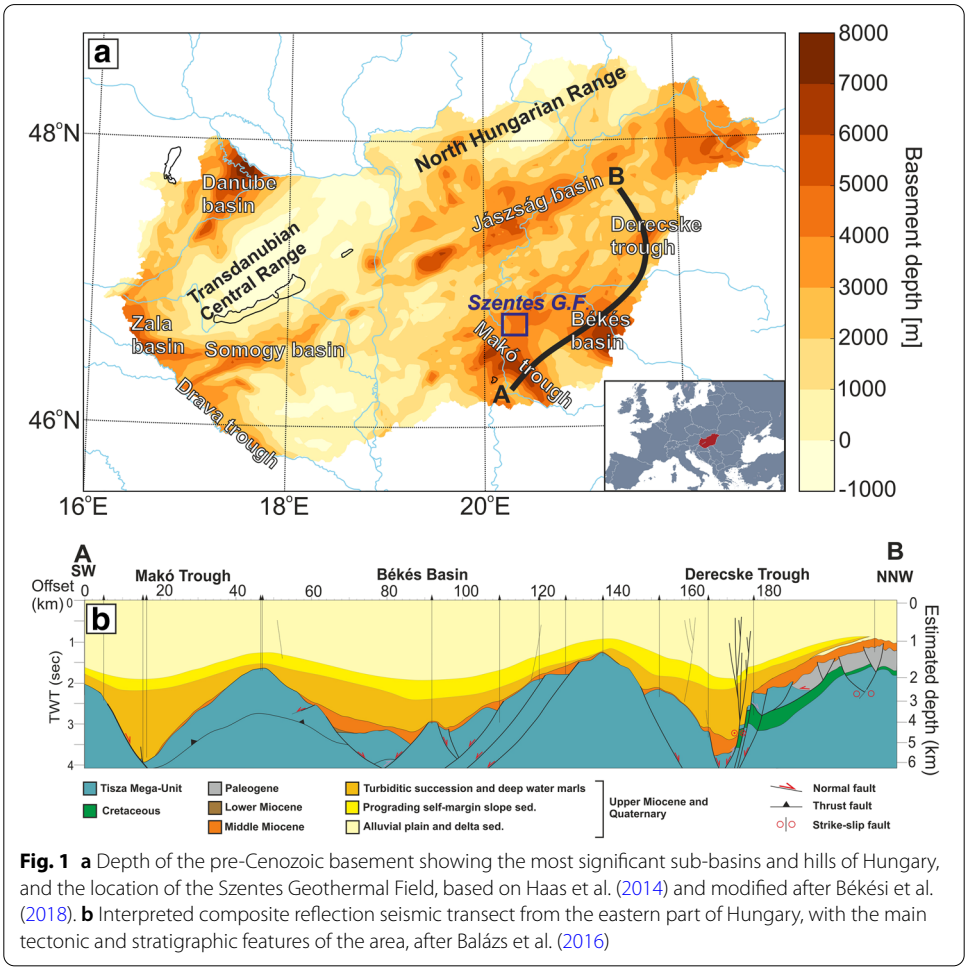

Fig. 1 **a** Depth of the pre-Cenozoic basement showing the most significant sub-basins and hills of Hungary, and the location of the Szentes Geothermal Field, based on Haas et al. (2014) and modified after Békési et al. (2018). **b** Interpreted composite reflection seismic transect from the eastern part of Hungary, with the main tectonic and stratigraphic features of the area, after Balázs et al. (2016)

Thermal water production in Hungary has already started in the nineteenth century for bathing purposes, and the country is still famous for its large amounts of hot springs and thermal spas. Geothermal wells most commonly target Upper Miocene and Quaternary porous sedimentary reservoirs (Fig. 1b). Fractured Mesozoic carbonate rocks also have significant geothermal potential, and are being utilized in several locations within Hungary (e.g., Goldscheider et al. 2010; Horváth et al. 2015; Mádl-Szőnyi et al. 2015; Szanyi and Kovács 2010). Additionally, fractured Mesozoic crystalline basement rock are also suitable targets for deep geothermal developments (e.g., Békési et al. 2018; Horváth et al. 2015; Vass et al. 2018), however, there has been no active exploitation of such resources yet. Until 2018, geothermal energy was exclusively used for direct heat purposes in Hungary. Since then, the first geothermal power plant has become operational in Tura, with an installed capacity of 3.35 MW_e (Nádor et al. 2019). Compared to its vast potential, Hungary is still lagging behind in geothermal energy production. Further geothermal developments are crucial to increase the role of renewable energy resources within Hungary's (and Europe's) energy demand. However, the long-term sustainable production of geothermal energy requires cautious planning and regulation. Exploitation in excess of natural recharge can result in reservoir pressure decline, causing a decrease in production rates. Furthermore, such "overexploitation" of geothermal reservoirs may lead to compaction, land subsidence, or even induced seismicity (e.g., Allis 2000; Békési et al. 2019; Keiding et al. 2010; Maghsoudi et al. 2018; Trugman et al. 2014; Meer et al. 2014).

Previous studies have demonstrated the effectiveness of interferometric synthetic aperture radar (InSAR) based monitoring combined with (inverse) modeling of geothermal fields (Heimlich et al. 2015; Keiding et al. 2010; Parks et al. 2020; Trugman et al. 2014; Vasco et al. 2013, 2002). In case of geothermal applications, inverse models constrained with ground motion data are commonly based on single or distributed volume/pressure sources in the subsurface (e.g., Kiyoo 1958; Okada 1985; Segall 2010; Yang et al. 1988). Ground deformation due to seismic events occurring at geothermal areas has also be modeled using analytical methods in order to estimate source parameters (e.g., Békési et al. 2021). More complex numerical models have also been applied to predict ground motions at geothermal sites. For instance, Vasco et al. (2013) applied coupled numerical modeling to resolve the observed ground deformation at the Geysers Geothermal Field. However, coupled models with large number of model parameters are not always suitable for inversion exercises incorporating extensive calibration datasets such as detailed surface movements as they require abundant runtime. The advantages of probabilistic ensemble-based approaches for inversion of surface subsidence have already been shown in several studies outside the geothermal energy arena (Baù et al. 2015; Candela et al. 2017; Fokker et al. 2016). Such ensemble-based approaches have limitations in terms of model parameters, including only a limited number of reservoir properties, and cannot directly distinguish between different subsurface processes. Still, ensemble-based techniques are capable of dealing with large amounts of measurements and they can successfully estimate driving parameters of subsurface processes. A recently developed ensemble-based subsidence interpretation and prediction tool (ESIP) is capable to distinguish between different compaction behaviors, and allows to predict a wide range of subsurface parameters (Candela et al. 2022). However, ESIP requires

detailed information on the local geology and pore pressure history of a study area for the whole operation period, that are not always available. In this study, we combine the Ensemble Smoother with Multiple Data Assimilation [ES-MDA, Emerick and Reynolds (2013)] with the analytical solution of Geertsma (1973), in order to estimate first-order properties of the Szentes geothermal area, without the requirement of high-resolution subsurface measurements, such as pressure time series. This study is the first application of mapping and modeling ground motions due to geothermal activities in Hungary, that aims to demonstrate the usefulness, requirements, and limitations of inverse geomechanical models for geothermal sites in Hungary and worldwide.

The Szentes geothermal field

The Szentes geothermal field is located in SE Hungary, in the northern part of the Makó trough (Fig. 1a). Upper Miocene delta front and delta plain sediments (Upper Pannonian Újfalu Formation) and delta top and alluvial plain sediments (Upper Pannonian Zagyva Formation) host the geothermal reservoir, deposited in the confines of a progradational delta system (e.g., Fig. 1b) (Juhász 1991; Sztanó et al. 2013). The targeted Upper Pannonian formations are largely heterogeneous; built up by the alternation of sandstone, silty sand, silty clay and clay layers (e.g., Juhász 1991). Geothermal production primarily targets the Újfalu formation, with a mean thickness of approximately 600 m in the vicinity of the geothermal wells, and a mean top depth of ~ 1500 m inferred from well logs. The individual sandstone layers have small lateral extent, therefore, it is difficult to correlate the sand bodies drilled in different wells. Still, hydraulic connection between the individual sand bodies exist. Natural pore pressure in the Upper Pannonian formations of the Szentes area is slightly above hydrostatic with a gradient of 10.2 MPa/km, however, extreme overpressure in the underlying Lower Pannonian strata (71 MPa/km) is observed (Bálint and Szanyi 2015). Such high overpressure in the low-permeability Lower Pannonian sediments is present in several locations of the Great Hungarian Plain, and most likely explained by tectonic processes (Almasi 2002; Tóth and Almási 2001; Balen and Cloetingh 1995).

Szentes is the first area where geothermal energy has been produced for industrial application in Hungary, with the first well drilled in 1958 (Bálint and Szanyi 2015; Szanyi and Kovács 2010). There are 45 wells drilled in total (including the Szegvár and Fábiánsebestyén areas), and 32 of them were producing thermal water up to 90 °C in 2010. Starting from the early 1970s, thermal water production reached ~ 6.5 million m^3/year, which has decreased to an average of 5.7 million m^3/year from the early 1990s (Szanyi and Kovács 2010). Yearly extracted thermal water volumes remained approximately constant after the early 1990s, although the exact yearly amounts cannot be precisely estimated due to the different owners of the individual wells, where production data are not always documented or provided. Additionally, geothermal wells have not been continuously operated; production during the summer period has been terminated in several wells. Yearly thermal water withdrawal has also slightly varied depending on winter temperatures. The complete lack of reinjection wells resulted in significant reservoir pressure decline and hydraulic head decrease with up to 36 m (Figs. 2a, b and 3). Reservoir pressures have started to increase since the mid-1990s due to the decrease in production rates in the western part of the geothermal filed, accompanied by 4–8 m

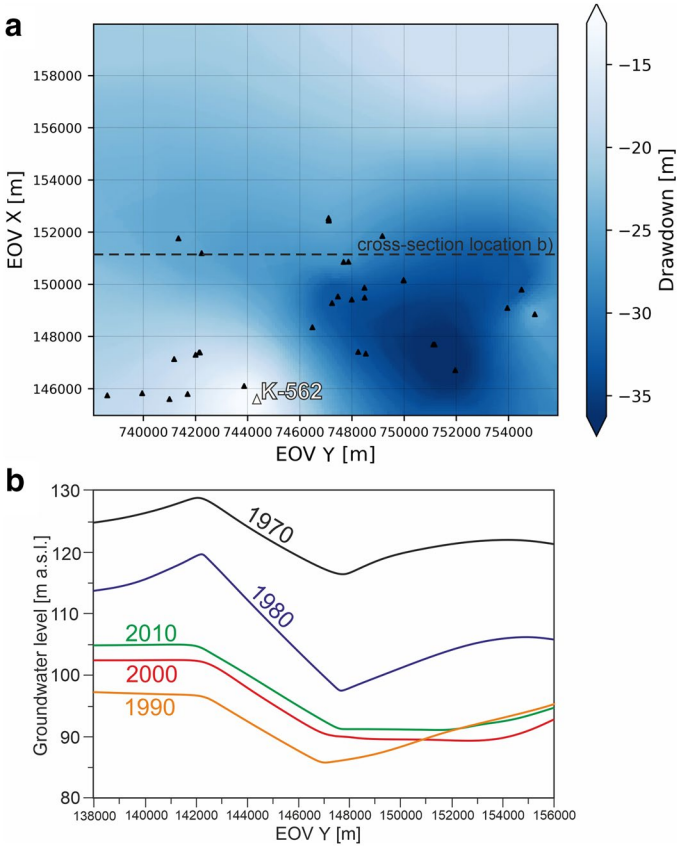

Fig. 2 **a** Drawdown measured at the bottom of the Upper Pannonian sequences at the Szentes geothermal field by 2000, and **b** cross-section showing the groundwater variations from 1970 to 2010, after Bálint and Szanyi (2015) and Szanyi and Kovács (2010). Please note that the original undisturbed water levels approximately agree with the estimated values for 1970. The largest decrease of hydraulic heads in 2000 occurred in the eastern part of the geothermal field, whereas hydraulic recovery of the western area has already started in the mid-1990s. The locations of well K-652 is labeled in **a** with white, where hydraulic head time series and InSAR-derived ground motions are plotted in Fig. 5

of hydraulic head increase by 2004 (Figure 4.2b, Szanyi et al. 2016; Szanyi and Kovács 2010). The largest drawdown occurred in the center of the field, with a decrease in hydraulic heads up to 36 m by 2000 (Fig. 2a, b) (Szanyi and Kovács 2010).

Regular monitoring of the Szentes geothermal wells from the beginning of thermal water withdrawal has not taken place, therefore, it is difficult to fully understand reservoir behavior through time. There are multiple factors responsible for the lack of regular measurements, for instance the different owners and operators of geothermal wells, inconsistencies in regulations of thermal water production in Hungary. We gathered downhole pressure measurements from the Szentes area (Fig. 3), showing that in some cases 2–3 decades passed between measurements. During 2009–2010, an investigation of 20 geothermal wells took place in the framework of the Jedlik project (Bálint and Szanyi 2015), including reliable downhole pressure measurements, showing that pore pressures were still below natural conditions in 2009–2010 (Fig. 3). Pore fluid pressures in 2010 were up to ~ 0.6 MPa lower than in 1980 (Fig. 3, yellow circles connected with a solid line), and depletion has probably reached its maximum in the early 1990s. Bálint

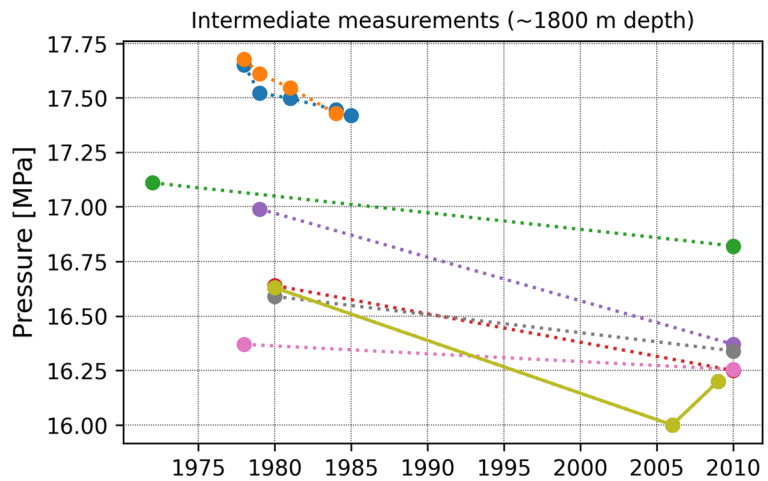

Fig. 3 Pore pressure measurements from the geothermal wells of Szentes after Bálint and Szanyi (2015), Szanyi et al. (2016) and the dataset of the Geo-Log Ltd. Measurements are plotted from ~ 1800 m depth. Different colors correspond to individual wells. Multiple observations from the same well are connected with a dotted line, however, these lines do not represent the pressure history. Pressure data from the well where the largest measured pressure decline occurred are represented with the yellow circles and solid lines

Table 1 Details of the SAR dataset that we selected for time series processing

InSAR data type	Track/frame number	Observation period	Number of scenes
Envisat descending	136/3697	November 2002–December 2006	14

and Szanyi (2015) studied the possible effect of reinjection towards a more sustainable field operation, by investigating the most suitable location and depth for an injection well. Since then reinjection in a single well has initiated, while production using downhole pumps is still ongoing.

InSAR data

We used C-band radar acquisitions of the European Space Agency's (ESA) Envisat satellites in order to map the ground motions for the period of November 2002–December 2006, summarized in Table 1. We assessed the availability and quality of radar images acquired on both ascending and descending satellite orbits. We introduced a criterion on the perpendicular baselines, and we discarded scenes with perpendicular baselines over 600 m, temporal baselines above 1 year and interferograms with no visual interferometric coherence. This criterion has reduced the number of scenes in case of both ascending and descending geometries, and we had to exclude the ascending images from further analysis due to the low number of scenes that we found insufficient for time series analysis.

To create the individual interferograms on the descending geometries, we used the ESA SNAP software (S1TBX—ESA Sentinel-1 Toolbox, http://step.esa.int). We applied orbital corrections on the individual scenes using DORIS Precise orbits. We selected a single master image using a criterion of minimizing the temporal and perpendicular baselines and we co-registered the images to the master geometry. We used the

1-arc-second (30 m) resolution Shuttle Radar Topography Mission Digital Elevation Model (SRTM DEM) to compute the topographic phase that we subsequently removed from the interferograms.

We obtained the time series of ground motions by Persistent Scatterer Interferometry (PSI), within the Matlab-based workflow of STAMPS (Hooper et al. 2007, 2012). In STAMPS, PS pixels are initially selected based on their amplitude dispersion, initially described by Ferretti et al. (2001). We selected a threshold of 0.4 for the amplitude dispersion index, allowing for a large number of pixels to be included in further analysis. Later, the number of PS was reduced during an iterative process based on phase stability. Interferograms were then corrected for spatially correlated and uncorrelated error terms as described by Hooper et al. (2012).

The PSI results indicate dominantly positive movements (~ uplift) at the Szentes geothermal field, with a deformation rate of ~ 5 mm/year (Fig. 4, outlined with a black rectangle) for the period of November 2002–December 2006. The largest positive LOS movements (~ uplift) is observed outside the geothermal field, in the north, with velocities up to 15 mm/year. Minor negative movements are observed south of the field, near the geothermal wells of Szegvár, and over the eastern and northeastern part of the Szentes field.

We plotted groundwater levels from well K-652 and LOS velocities of PS pixels within 500 m distance from the well (Fig. 5). Hydraulic head measurements from the Szentes area are rather limited; well K-652 was chosen because it has the most frequent observation history, and covers the duration of the InSAR monitoring. Hydraulic head data in the

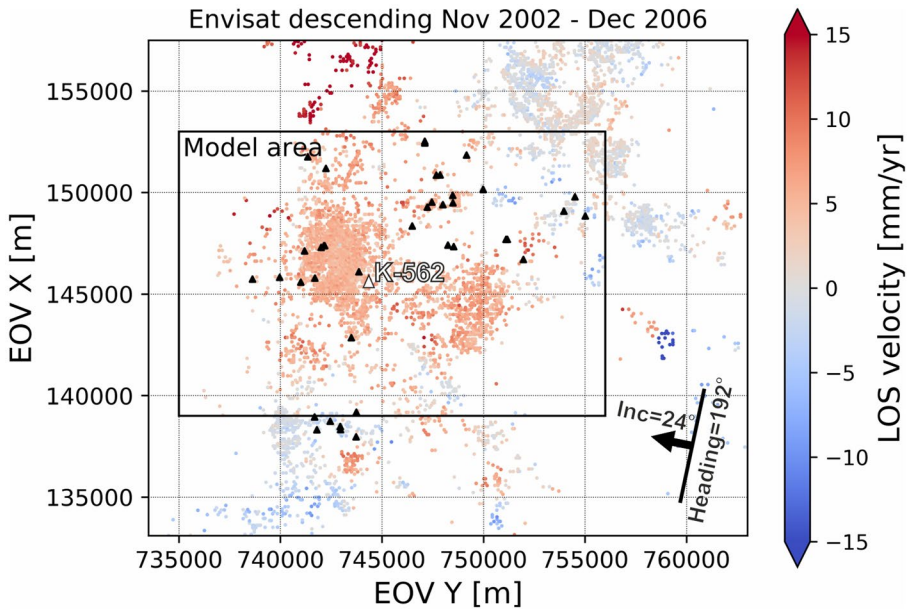

Fig. 4 Mean LOS velocities estimated for descending satellite orbits, for the period of ~ 4 years (November 2002–December 2006). Negative LOS velocities indicate movement away from the satellite (~ subsidence) and positive values show movement towards the satellite (~ uplift). Arrows indicate the flight direction of the satellite and the look direction with the corresponding incidence angles. The locations of the geothermal wells are plotted with black triangles. The modeling area that corresponds to the Szentes geothermal filed, excluding the Szegvár thermal wells that are located south of the field, is outlined with black rectangle

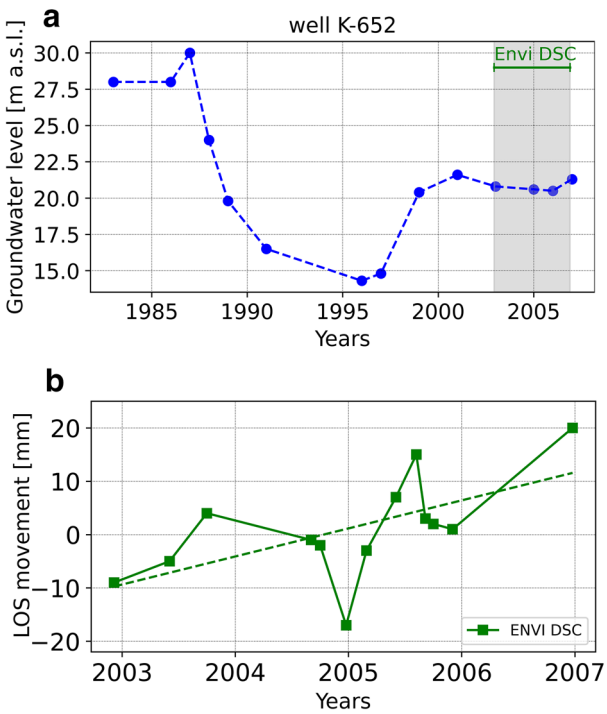

Fig. 5 Hydraulic head measurements (**a**) and PS-InSAR time series of descending satellite orbits (**b**) in/near well K-652 located in the southern part of the Szentes geothermal field. For the InSAR time series plot, PS points within 500 m distance from well K-652, with a standard deviation < 2 mm/year are included. For the location of the geothermal well, see Figs. 2 and 4

K-652 well, located in the southern part of the geothermal field, show a decreasing trend until 1995, when the recovery of water levels started (Fig. 5a). The InSAR time series can be approximated with a linear trend (Fig. 5b), with 2 major negative and positive deviation in ~ January 2005 and August 2005. These anomalies might be explained by the fact that thermal water production was terminated for the summer period, allowing for the short-term recovery of groundwater levels. In the vicinity of well K-652, the InSAR measurements indicate positive LOS motions (~ uplift) of the area, although groundwater levels do not show any significant variation (only a minor increase of 0.5 m) between 2002 and 2007 (Fig. 5a). It is important to note that InSAR observations are averaged within 500 m distance of the geothermal well and the open sections of the geothermal well only partly cover the vertical extent of the geothermal reservoir, since the aquifer units are separated with clay-rich aquitards with variable thickness and depth. Formation pressures might be different away from the boreholes, as the initially artesian wells required pumping after several years of production, when water levels declined and no longer reached the ground surface. If pressure changes are restricted to certain parts of the reservoir, the measured groundwater levels may not reflect these changes that might explain the discrepancies between the observed groundwater levels and LOS movements.

Inverse geomechanical modeling

We modeled ground movements using the analytical solution of Geertsma (1973), for a disk-shaped reservoir undergoing a uniform pore pressure increase/decline, embedded in a homogeneous elastic half-space, with a Poisson's ratio ν. In the Geertsma model, the vertical (u_z) and radial (u_r) components of movements at the surface due to pressure change, Δp., attributed to a disk-shaped source with radius, R, and height, h, compaction coefficient or compressibility, c_m, and burial depth, D, can be obtained as (Geertsma 1973):

$$u_z(r,\ \ 0) = 2(1-\nu)c_m h\Delta pR \int_0^\infty e^{-D\alpha} J_1(\alpha R) J_0(\alpha r) d\alpha, \tag{1}$$

$$u_r(r,\ \ 0) = 2(1-\nu)c_m h\Delta pR \int_0^\infty e^{-D\alpha} J_1(\alpha R) J_1(\alpha r) d\alpha, \tag{2}$$

where e is the Euler's number, J_0 and J_1 are first-type Bessel functions of order 0 and 1, respectively, and r is the distance measured from the center of the source. The formula can be simplified by substituting $c_m h\Delta p = \Delta h$, where Δh is the height change of the reservoir. This simple model cannot take into account complex geological settings and variations in subsurface geomechanical and petrophysical properties, but it can be efficient for a first approximation of ground deformation induced by injection/production activities. Due to its simplicity, the driving parameters of the Geertsma model can be estimated in a computationally inexpensive way by inversion techniques. Estimates of reservoir parameters and related uncertainties, for instance the compressibility, is highly relevant for more complex 3D reservoir models, to increase their reliability by choosing reasonable input parameters.

For the modeling of ground deformation, we selected an area of approximately 20×15 km outlined in Fig. 4, based on the observed surface movements and well locations at Szentes. We excluded the southernmost geothermal wells of Szegvár and the location of a major positive ground motion anomaly outside the geothermal field in the north (Fig. 4) from the modeling. It was necessary since the modeled ground motion pattern would have been too complex to capture the major ground motion anomalies that occur in the vicinity of the Szentes geothermal wells with a simple model. We primarily concentrated on the major positive LOS anomaly identified on descending satellite orbits for the period of November 2002 and December 2006 (Fig. 4). We first tested the model with one single Geertsma source with uniform pressure increase (source 1), selecting broad prior ranges of model parameters. We assumed a uniform pressure increase based on the InSAR observations and the hydraulic head profile (Fig. 2b), indicating increasing groundwater levels at the bottom of the geothermal reservoir (base of the Újfalu formation). Having only one source, an unmapped negative LOS anomaly remained ~ east of the main uplift signal (Fig. 6b, e). To account for this subsidence, we included an additional small source with negative pressure change (source 2) to the model (Fig. 6a, c) based on the InSAR measurements.

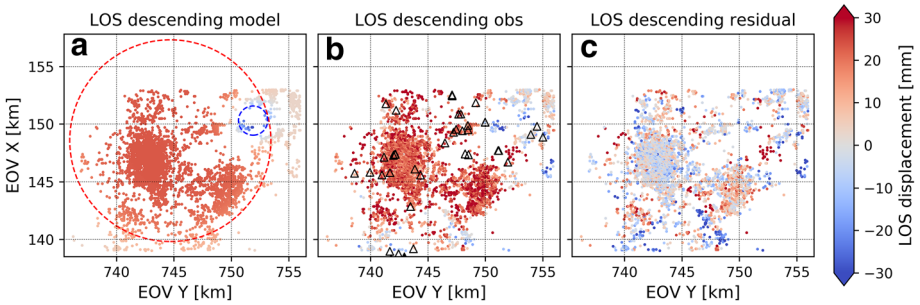

Fig. 6 Modeled (**a**), observed (**b**), and residual (**c**) displacements in the LOS direction observed on the descending satellite pass. Red and blue dotted circles in **a** show the locations of the best fitting Geertsma sources, using the mean values from the posterior model run. The large, red circle corresponds to the positive pressure source that is responsible for the major uplift signal, and the small blue circle accounts for pressure decrease in the eastern part of the geothermal field

To estimate the model parameters and uncertainties, we applied ensemble-based probabilistic inversion, having the ascending and descending InSAR datasets as target observations. The Ensemble Smoother [ES, Emerick and Reynolds (2013)] estimates the model parameters by a global update, incorporating all data available. Therefore, inverse problems with large number of observations can be solved by the ES in a computationally efficient way. For non-linear forward models, the ES requires several iterations, where the predictions of the previous run is used as an input for the subsequent data assimilation step (ES-MDA, Emerick and Reynolds 2013). In case of the forward model based on the analytical solution of Geertsma (1973), only a weak nonlinearity between ground motion and certain model parameters (radius and depth of the disk-shaped sources) exist. Still, we choose ES-MDA as we expected a better performance than a single ES and to be able to evaluate the improvement of the solution with each DA steps.

The solution for a single data assimilation for the updated model ensemble is:

$$\hat{M} = M + M'[\mathrm{GM}']^{\mathrm{T}}\left\{\mathrm{GM}'[\mathrm{GM}']^{\mathrm{T}} + (N_e - 1)C_d^{-1}\right\}^{-1} \times (D - \mathrm{GM}). \tag{3}$$

In Eq. 3, M is the prior ensemble of model parameters, GM represents the result of the forward model working on all ensemble members, and GM′ is the difference between GM and its mean. N_e is the number of ensembles, and D is an ensemble of data realizations, created by perturbing the measurements according to their covariance matrix (C_d). The mean of the ensemble is taken as the best estimate, which is used as input for the next update in case of ES-MDA. The number of data assimilation steps, N_a must be selected a priori. The data covariances used for the update steps are increased by a multiplication factor, α_i for $i = 1, 2\ldots, N_a$, and α_i must be selected as $\sum_{i=1}^{N_a} \frac{1}{\alpha_i} = 1$ (Emerick and Reynolds 2013). This is necessary to compensate for the effect of multiple application of an ES.

For the inverse modeling with ES-MDA, we fixed the depth of the sources to 1500 m, which was identified as the mean depth of the top of the reservoir from well logs and seismic data. We approximated the subsurface with an elastic half-space, with a Poisson's ratio $\nu = 0.28$, that we selected based on average values for the area inferred from well logs. The model parameters include the location (X and Y), radius (R) and height change

(Δh) of the two disk-shaped sources, 8 parameters in total. We assigned prior values for the parameters assuming normal distribution, except for the height change of both sources, where a lognormal distribution was chosen (Table 2). We selected prior values for the height change to be positive in case of source 1, accounting for a positive pressure change at depth attributed to the major positive LOS displacement anomaly. The height change of source 2 was assumed to be negative, approximating pressure decline and corresponding subsidence. Measurement errors of the InSAR observations were set to 4 mm, after testing the influence of different values (2–8 mm) on the inversion procedure. We first included only one source in the parameter estimation procedure allowing for broad prior values, to get a first-pass model for the major positive pressure source. Using the mean posterior model parameters of the one source model, we estimated the parameters of the second source combined with the first source having fixed parameters. We iteratively fixed one source at a time, until no significant improvement compared to the previous model was achieved. Then, we assigned relatively narrow ranges to the prior parameters, with mean and standard deviation reported in Table 2. Having these prior statistics, we estimated all model parameters of the two sources through the same ES-MDA run, using all InSAR observations. The data assimilation procedure was performed with 100 ensemble members and 4 iterations or data assimilation steps.

Modeling results indicate the presence of an extensive positive pressure source, with a radius of 8755 ± 38 m (source 1, red dashed circle in Fig. 6a), and a smaller negative source with a radius of 1269 ± 34 m (source 2, blue dashed circle in Fig. 6a). Source 1 is located at the center of the Szentes geothermal field, covering the locations of most of the geothermal wells. The location of source 2 corresponds to the vicinity of production wells in the eastern part of the field. Source 2 is positioned almost entirely inside the large positive source (Fig. 6a), suggesting that source 2 is superimposed on top of the significantly larger source 1.

Table 2 List of the model parameters and their prior and posterior statistics

Parameter (unit)	Symbol	Prior statistics		Posterior statistics	
		Mean	Standard deviation	Mean	Standard deviation
X coordinate of source 1 (m)	X_1	$\mu_{X_1} = 744{,}500$	$\sigma_{X_1} = 1000$	$\mu_{X_1} = 744{,}690$	$\sigma_{X_1} = 38.0$
Y coordinate of source 1 (m)	Y_1	$\mu_{Y_1} = 146{,}500$	$\sigma_{Y_1} = 1000$	$\mu_{Y_1} = 148{,}569$	$\sigma_{Y_1} = 53.7$
Radius of source 1 (m)	R_1	$\mu_{R_1} = 7000$	$\sigma_{R_1} = 500$	$\mu_{R_1} = 8755$	$\sigma_{R_1} = 44.6$
Height change of source 1 (m)	Δh_1	$\mu_{\log(\Delta h1)} = -3.9$	$\sigma_{\log(\Delta h1)} = 0.18$	$\mu_{\log(\Delta h1)} = -3.88$	$\sigma_{\log(\Delta h1)} = 0.0023$
X coordinate of source 2 [m]	X_2	$\mu_{X_2} = 751{,}800$	$\sigma_{X_2} = 300$	$\mu_{X_2} = 751{,}893$	$\sigma_{X_2} = 15.3$
Y coordinate of source 2 (m)	Y_2	$\mu_{Y_2} = 150{,}000$	$\sigma_{Y_2} = 300$	$\mu_{Y_2} = 150{,}300$	$\sigma_{Y_2} = 12.3$
Radius of source 2 (m)	R_2	$\mu_{R_2} = 1000$	$\sigma_{R_2} = 100$	$\mu_{R_2} = 1269$	$\sigma_{R_2} = 34.1$
Height change of source 2 (m)	Δh_2	$\mu_{\log(-\Delta h2)} = -2.0$	$\sigma_{\log(-\Delta h2)} = 0.14$	$\mu_{\log(-\Delta h2)} = -1.66$	$\sigma_{\log(-\Delta h2)} = 0.05$

The model can adequately approximate the major structures of the ground motion observations (Fig. 6). Still, residual surface movements (Fig. 6c) are significant at certain areas, suggesting that the simple model could not entirely reproduce the InSAR time series displacements. The overall RMSE of the model is 7.5 mm. The average observed displacements in the model area is 20.3 mm with a maximum of 59 mm, and only 9% of the observations show movements > 30 mm. The average modeled displacement is 20.38, which is almost identical with the observed one, while the maximum modeled movement is 23.4 mm, which is significantly smaller than the observed maximum value. Local ground motion anomalies with large displacements (> 30 mm) can explain the relatively large RMSE, showing that the complexity of the subsurface cannot be captured by the model. Still, the motivation for such simple model was to have an estimate on the sources that are responsible for the major pattern of ground movements and to find reasonable intervals for compaction coefficients that are mapped within Δh_1 and Δh_2 and related uncertainties of the reservoir system.

The resulting posterior model parameters and their standard deviations suggest that all model parameters are well constrained compared to their prior statistics (Table 2, Fig. 7). Figure 7 demonstrates the improvement of the uncertainties of model parameters through each data assimilation run. No clear correlation between model parameters have been identified except for the height change (Δh_2) and the radius (R_2) of source 2 (Fig. 7d). The correlation between Δh_2 and R_2 is clearly shown by Fig. 8, identified as a linear relationship between the logarithm of the parameters with a slope close to − 0.5. Apparently, all posterior parameters can be constrained independently,

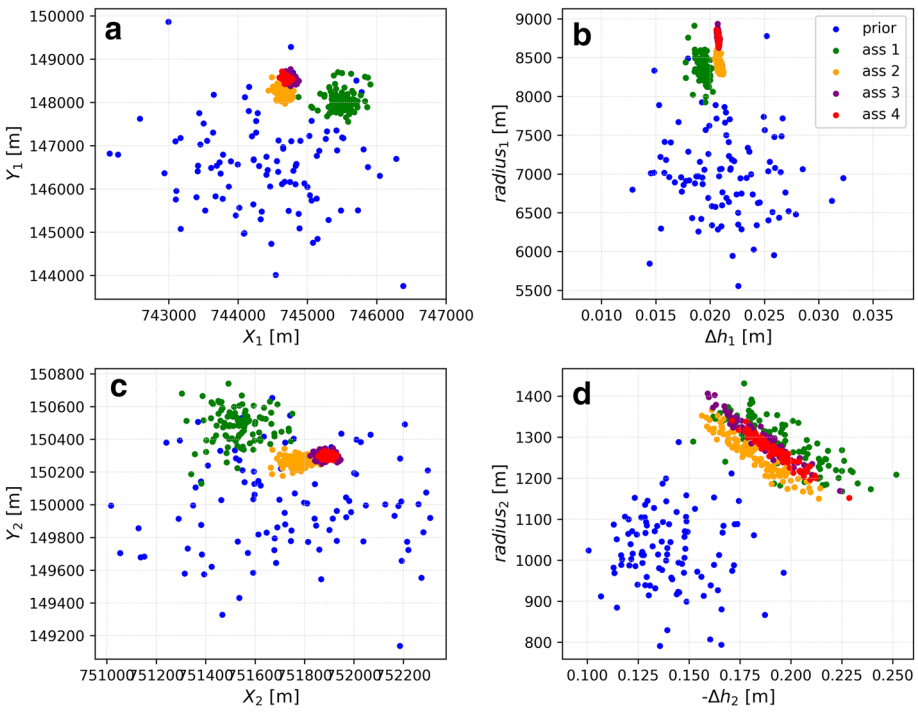

Fig. 7 Prior (blue circles) and posterior ensembles of the model parameters for source 1 (**a**, **b**) and source 2 (**c**, **d**), including all 4 data assimilation steps. The final parameters are shown with red circles

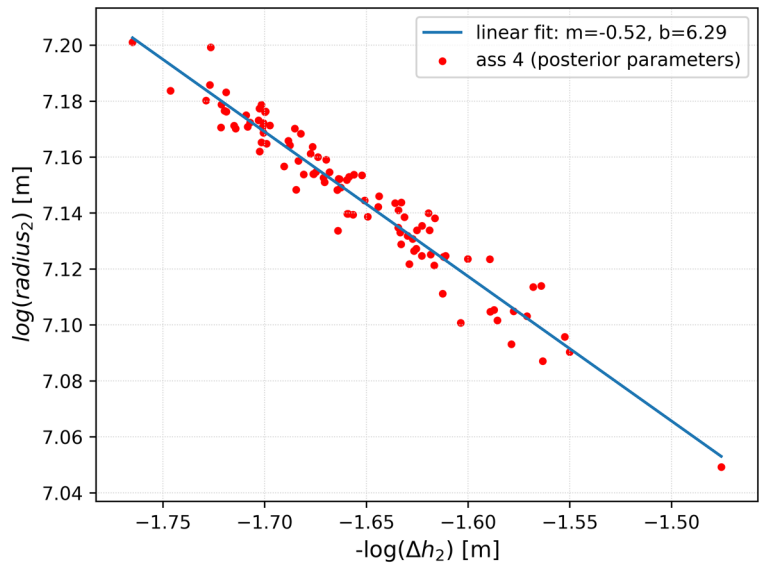

Fig. 8 Plot showing the correlation between the logarithm of the height change (Δh_2) and the radius (R_2) of the small compaction source (source 2), and corresponding parameters of the linear fit

but the product $\Delta h_2 R^2$ can be estimated better than the two parameters separately. This is related to the fact that the subsidence of a relatively small source is in first order proportional to its compacting volume, for which $\pi \Delta h_2 R^2$ is the measure.

Discussion

PS-InSAR time series of ground deformation together with the modeling results suggest that uplift of the Szentes geothermal field due to pore pressure recovery occurred between November 2002 and December 2006. Since no injection wells were operated at Szentes before 2018, and production temperatures remained relatively constant through the entire production period (Bálint and Szanyi 2015), we explain ground uplift with pore pressure increase due to natural recharge. The inferred pressure recovery of the Szentes geothermal area is in agreement with increasing water levels measured at the bottom of the Upper Miocene (Upper Pannonian) sediments between 2000 and 2010 by Bálint and Szanyi (2015) (Fig. 2b). Additionally, on top of the recharge of the whole area, subsidence of the northeastern part of the geothermal field is observed, although pressure and groundwater level measurements indicating pressure decline in the reservoir are not available.

With the Geertsma models for surface displacement due to two disk-shaped reservoirs embedded in an elastic half-space with uniform pressure increase and decline, we managed to reproduce the major anomalies observed on the ground movement maps (Fig. 6). However, significant misfits between observed and modeled surface deformation remained at certain locations (Fig. 6c). We attribute those to the limitations of the model, assuming constant reservoir properties and a perfectly circular shape. As a matter of fact, sedimentation in the Makó trough followed aggradational

and progradational cycles, with various lithologies (e.g., Sztanó et al. 2013). The resulting local variations in sand and clay content of the reservoir cause heterogeneous properties, most importantly a highly variable compaction coefficient, causing variations in the magnitude of ground deformation mapped with InSAR.

The formula of Geertsma (1973) shows a linear relationship between ground motion and the product of reservoir compaction coefficient, reservoir height, and pressure change. Inversion techniques fail to constrain each of these parameters individually. Therefore, we constrained the product of the three parameters of both sources (Table 2 Fig. 7). Then, we plotted the decompaction coefficient associated with the source 1 as a function of reservoir pressure, with constant reservoir heights of 200, 400 and 600 m (Fig. 9), based on the mean posterior products of the three parameters (Δh_1). We outlined intervals with reasonable values for pressure change based on water level variations for the section in Fig. 2b, groundwater level measurements in well K-652. The inferred decompaction coefficient of source 1 varies between ~ 0.2 and 2×10^{-9} Pa^{-1} (Fig. 9), characterizing the elastic behavior of the Szentes geothermal reservoir.

The compaction coefficient attributed to the small source with pressure decline was not assessed due to the lack of pressure/groundwater level measurement supporting the pressure decline that could explain the observed subsidence, and the correlation between the radius and the height change of source 2, as shown in Figs. 7d, 8.

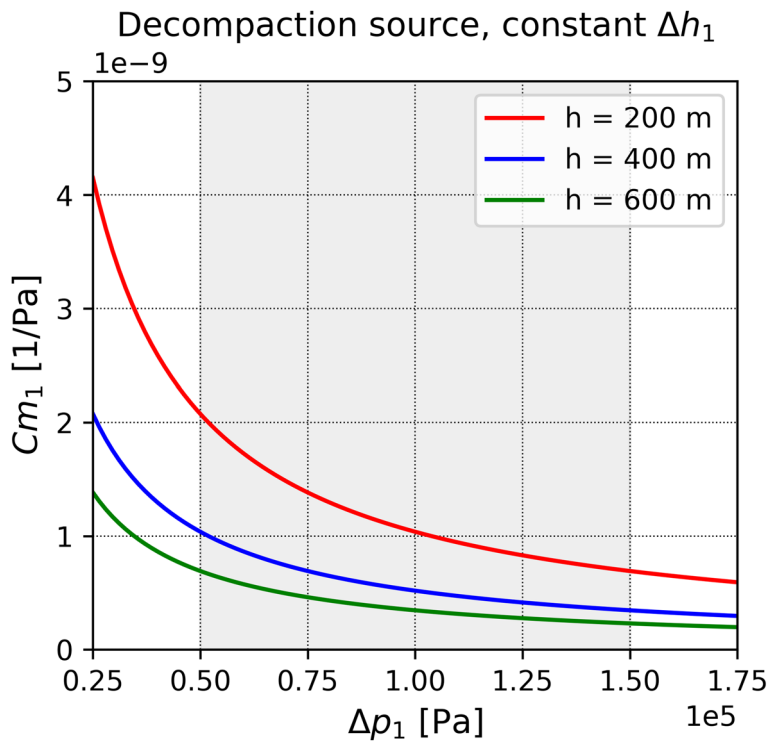

Fig. 9 Decompaction coefficient associated with sources 1 as a function of reservoir pressure, with constant reservoir heights of 200, 400 and 600 m. The interval with reasonable values for pressure change based on water level observations from the locations of the corresponding source is outlined with grey. C_m values that lie within the grey interval indicate reasonable estimates for the decompaction coefficients of the reservoir system

We attempted to compare the resulting decompaction coefficient attributed to the Upper Pannonian sediments with a porosity of 21–28% at Szentes with various sandstones worldwide, to reveal if the resulting values are realistic. We only made comparisons with compaction coefficients of sandstones that were inferred from ground deformation observations. For instance, Thienen-Visser et al. (2015) estimated the compaction coefficient of the Rotliegend sandstones in the Groningen gas field with porosities of 12–22% to a maximum value of 2×10^{-10} Pa^{-1}. This value agrees with the lower limit of the inferred decompaction coefficient estimated for the Upper Pannonian sandstones in Szentes. Since the lower limit of reservoir porosity in Szentes (21%) is almost identical with upper limit of the porosity of the Rotliegend sandstone in Groningen (22%), we can conclude that our estimates are realistic.

The decompaction coefficient of the Szentes reservoir system may be different from the compaction coefficient corresponding to the earlier depressurization periods, as the water-bearing sand bodies are often separated with aquitards composed of clay layers that often experience permanent, irreversible compaction (e.g., Pijnenburg et al. 2019). The individual compaction coefficient of clays are considered to be significantly higher than the sand bodies (e.g., Zimmerman 1990). As a result, they could contribute significantly to the overall compaction coefficient of the reservoir system. The compaction of aquitards may be responsible for the observed local subsidence in the northeastern part of the field, although this hypothesis is not supported by any pressure/groundwater level measurements. Compaction of highly compressible lithologies (mudstones) were identified as main sources of ground subsidence for instance at the Wairakei–Tauhara and Ohaaki geothermal areas in New Zealand, with up to 15 m (Hole et al. 2007). To properly assess the contributions of elastic and inelastic deformation at the study area and fully understand the compaction behavior of the reservoir, ground deformation observations and more frequent pressure measurements of the major depletion period are required.

Conclusions

We performed PS-InSAR time series analysis of Envisat SAR images acquired on descending satellite tracks, for the period of November 2002–December 2006, covering the Szentes geothermal area in SE Hungary. The ground movement observations were used in inverse models based on the analytical function of Geertsma (1973), for ground deformation induced by a constant pressure change in a cylindrical source at depth. We constrained the model parameters with an ensemble smoother with multiple data assimilation and we managed to reproduce the main features of the observed surface movements with the combination of a larger source with positive pressure change, and a smaller depleting source. The procedure yielded reasonable estimates of the model parameters and their uncertainties.

Ground movements together with the modeling results suggest that uplift of the Szentes geothermal field occurred between November 2002 and December 2006, which is explained by pore pressure recovery supported by natural recharge. Based on the InSAR data, inverse modeling, and groundwater level variations, we managed to provide reasonable estimates on the decompaction coefficient of the reservoir ($\sim 0.2 \times 10$–9–2.0×10^{-9} Pa^{-1}), characterizing the elastic behavior of the sandstone

aquifers. Additionally, permanent compaction of aquitards represented by imbedded clay layers of the reservoir system may have occurred during the earlier depressurization period, from ~ 1970 to the mid-1990s. Compaction of aquitards may have continued in the northeastern part of the field, where a minor negative ground motion anomaly is observed.

The InSAR surface movement estimates, employed in an ES-MDA inverse modeling scheme, have shown to combine to an efficient tool to make a first-order estimate of the properties and processes at the Szentes geothermal area. The inferred properties and processes are highly relevant as an input of more complex reservoir models and for predictions for future production scenarios, targeting a sustainable production plan. To achieve more reliable estimates on the reservoir behavior, ground motion observation of the entire thermal water extraction period, and more frequent pressure/hydraulic head measurements would be required. Future projects combining InSAR with forward and inverse modeling with high-resolution subsurface datasets potentially have an important role in in the sustainable exploitation of the highly prospective geothermal resources in the Pannonian Basin.

Abbreviations

InSAR: Interferometric synthetic aperture radar; ES-MDA: Ensemble smoother with multiple data assimilation; PSI: Persistent scatterer interferometry.

Acknowledgements

We thank Kristóf Porkoláb for providing writing suggestions.

Authors' contributions

EB: conceptualization, design, analysis of the data, interpretation, writing the manuscript. PF: design, interpretation, supervision, revising the manuscript. TC: design, interpretation, revising the manuscript. JSZ: interpretation, revising the manuscript. JDW: interpretation, supervision, revising the manuscript. All authors read and approved the final manuscript.

Funding

The research leading to these results has received funding from the GEMex Project, funded by the European Union's Horizon 2020 research and innovation programme under Grant Agreement No. 727550.

Availability of data and materials

Envisat satellite datasets analyzed during the current study are accessible through the EO-CAT Earth Observation Catalogue (https://eocat.esa.int) after registration.

Declarations

Competing interests

The authors declare that they have no known competing financial interests or personal relationships that could have appeared to influence the work reported in this paper.

Author details

[1]Utrecht University, 3584 CB Utrecht, Netherlands. [2]Institute of Earth Physics and Space Science, Csatkai E. u. 6–8., Sopron, Hungary. [3]TNO Utrecht, 3584 CB Utrecht, Netherlands. [4]University of Szeged, Egyetem u. 2., Szeged, Hungary.

Received: 14 July 2021 Accepted: 1 March 2022
Published online: 15 March 2022

References

Allis RG. Review of subsidence at Wairakei field, New Zealand. Geothermics. 2000;29(4–5):455–78.
Almasi I. Petroleum hydrogeology of the Great Hungarian Plain, Eastern Pannonian Basin, Hungary. Edmonton: University of Alberta; 2002.
Bada G, Horváth F, Dövényi P, Szafián P, Windhoffer G, Cloetingh S. Present-day stress field and tectonic inversion in the Pannonian basin. Global Planet Change. 2007;58(1–4):165–80.
Balázs A, Matenco L, Magyar I, Horváth F, Cloetingh S. The link between tectonics and sedimentation in back-arc basins: new genetic constraints from the analysis of the Pannonian Basin. Tectonics. 2016;35(6):1526–59.

Bálint A, Szanyi J. A half century of reservoir property changes in the Szentes geothermal field, Hungary. Cent Eur Geol. 2015;58(1–2):28–49.
Baù D, Ferronato M, Gambolati G, Teatini P, Alzraiee A. Ensemble smoothing of land subsidence measurements for reservoir geomechanical characterization. Int J Numer Anal Meth Geomech. 2015;39(2):207–28.
Békési E, Lenkey L, Limberger J, Porkoláb K, Balázs A, Bonté D, Vrijlandt M, Horváth F, Cloetingh S, van Wees J-D. Subsurface temperature model of the Hungarian part of the Pannonian Basin. Glob Planet Change. 2018;171:48–64.
Békési E, Fokker PA, Martins JE, Limberger J, Bonté D, Van Wees J-D. Production-induced subsidence at the Los Humeros geothermal field inferred from PS-InSAR. Geofluids. 2019;2019:12.
Békési E, Fokker PA, Martins JE, Norini G, van Wees J-D. Source parameters of the 8 February 2016, Mw = 4.2 Los Humeros earthquake by the inversion of InSAR-based ground deformation. Geothermics. 2021;94:102133.
Candela T, Osinga S, van der Veer E, der Heege J, Fokker P. Improving reservoir exploitation using fast geomechanical modelling coupled with surface displacement data assimilation. In: Proceedings SPE reservoir characterisation and simulation conference and exhibition. Dallas: Society of Petroleum Engineers; 2017.
Candela T, Chitu A, Peters E, Pluymaekers M, Hegen D, Koster K, Fokker P. Subsidence induced by gas extraction: a data assimilation framework to constrain the driving rock compaction process. Frontiers in Earth Science - Solid Earth Geophysics; 2022 (**in press**).
Cloetingh S, Van Wees JD, Ziegler P, Lenkey L, Beekman F, Tesauro M, Förster A, Norden B, Kaban M, Hardebol N. Lithosphere tectonics and thermo-mechanical properties: an integrated modelling approach for Enhanced Geothermal Systems exploration in Europe. Earth Sci Rev. 2010;102(3–4):159–206.
Emerick AA, Reynolds AC. Ensemble smoother with multiple data assimilation. Comput Geosci. 2013;55:3–15.
Ferretti A, Prati C, Rocca F. Permanent scatterers in SAR interferometry. IEEE Transact Geosci Remote Sens. 2001;39(1):8–20.
Fokker P, Wassing B, Van Leijen F, Hanssen R, Nieuwland D. Application of an ensemble smoother with multiple data assimilation to the Bergermeer gas field, using PS-InSAR. Geomech Energy Environ. 2016;5:16–28.
Geertsma J. Land subsidence above compacting oil and gas reservoirs. J Pet Technol. 1973;25(06):734–44.
Goldscheider N, Mádl-Szőnyi J, Erőss A, Schill E. Thermal water resources in carbonate rock aquifers. Hydrogeol J. 2010;18(6):1303–18.
Haas J, Budai T, Csontos L, Fodor L, Konrád G, Koroknai B. Geology of the pre-Cenozoic basement of Hungary. Budapest: Geological and Geophysical Institute of Hungary; 2014. p. 1–71.
Heimlich C, Gourmelen N, Masson F, Schmittbuhl J, Kim S-W, Azzola J. Uplift around the geothermal power plant of Landau (Germany) as observed by InSAR monitoring. Geotherm Energy. 2015;3(1):1–12.
Hole J, Bromley C, Stevens N, Wadge G. Subsidence in the geothermal fields of the Taupo Volcanic Zone, New Zealand from 1996 to 2005 measured by InSAR. J Volcanol Geotherm Res. 2007;166(3–4):125–46.
Hooper A, Segall P, Zebker H. Persistent scatterer interferometric synthetic aperture radar for crustal deformation analysis, with application to Volcán Alcedo, Galápagos. J Geophys Res Solid Earth. 2007. https://doi.org/10.1029/2006JB004763.
Hooper A, Bekaert D, Spaans K, Arıkan M. Recent advances in SAR interferometry time series analysis for measuring crustal deformation. Tectonophysics. 2012;514:1–13.
Horváth F. Towards a mechanical model for the formation of the Pannonian basin. Tectonophysics. 1993;226(1–4):333–57.
Horváth F, Cloetingh S. Stress-induced late stage subsidence anomalies in the Pannonian Basin. Tectonophysics. 1996;266:287–300.
Horváth F, Bada G, Szafián P, Tari G, Ádám A, Cloetingh S. Formation and deformation of the Pannonian Basin: constraints from observational data. Geol Soc. 2006;32(1):191–206.
Horváth F, Musitz B, Balázs A, Végh A, Uhrin A, Nádor A, Koroknai B, Pap N, Tóth T, Wórum G. Evolution of the Pannonian basin and its geothermal resources. Geothermics. 2015;53:328–52.
Juhász G. Lithostratigraphical and sedimentological framework of the Pannonian (sl) sedimentary sequence in the Hungarian Plain (Alföld), Eastern Hungary. Acta Geol Hung. 1991;34(1–2):53–72.
Keiding M, Árnadóttir T, Jónsson S, Decriem J, Hooper A. Plate boundary deformation and man-made subsidence around geothermal fields on the Reykjanes Peninsula, Iceland. J Volcanol Geotherm Res. 2010;194(4):139–49.
Kiyoo M. Relations between the eruptions of various volcanoes and the deformations of the ground surfaces around them. Earthq Res Inst. 1958;36:99–134.
Lenkey L, Dövényi P, Horváth F, Cloetingh S. Geothermics of the Pannonian basin and its bearing on the neotectonics, vol. 3. Western Chukotka: EGU Stephan Mueller Special Publication Series; 2002. p. 29–40.
Lenkey L, Mihályka J, Paróczi P. Review of geothermal conditions of Hungary. Földt Közlöny. 2021;151(1):65–65.
Limberger J, Calcagno P, Manzella A, Trumpy E, Boxem T, Pluymaekers M, van Wees J-D. Assessing the prospective resource base for enhanced geothermal systems in Europe. Geotherm Energy Sci. 2014;2(1):55–71.
Limberger J, van Wees J-D, Tesauro M, Smit J, Bonté D, Békési E, Pluymaekers M, Struijk M, Vrijlandt M, Beekman F. Refining the thermal structure of the European lithosphere by inversion of subsurface temperature data. Glob Planet Change. 2018;171:18–47.
Mádl-Szőnyi J, Pulay E, Tóth Á, Bodor P. Regional underpressure: a factor of uncertainty in the geothermal exploration of deep carbonates, Gödöllő Region, Hungary. Environ Earth Sci. 2015;74(12):7523–38.
Maghsoudi Y, van der Meer F, Hecker C, Perissin D, Saepuloh A. Using PS-InSAR to detect surface deformation in geothermal areas of West Java in Indonesia. Int J Appl Earth Obs Geoinf. 2018;64:386–96.
Nádor A, Kujbus A, Tóth A. Geothermal energy use, country update for Hungary. Den Haag: European Geothermal Congress; 2019.
Okada Y. Surface deformation due to shear and tensile faults in a half-space. Bull Seismol Soc Am. 1985;75(4):1135–54.
Parks M, Sigmundsson F, Sigurðsson Ó, Hooper A, Hreinsdóttir S, Ófeigsson B, Michalczewska K. Deformation due to geothermal exploitation at Reykjanes, Iceland. J Volcanol Geotherm Res. 2020;391:106438.
Pijnenburg R, Verberne B, Hangx S, Spiers C. Intergranular clay films control inelastic deformation in the Groningen gas reservoir: evidence from split-cylinder deformation tests. J Geophy Res Solid Earth. 2019;124(12):12679–702.
Segall P. Earthquake and volcano deformation. Princeton: Princeton University Press; 2010.
Szanyi J, Kovács B. Utilization of geothermal systems in South-East Hungary. Geothermics. 2010;39(4):357–64.

Szanyi J, Bálint A, Osvald M, Kovács B, Czinkota I, Nagygál J. Sustainability of Szentes geothermal field operations. Bucuresti: Asociatia Hidrogeologilor din Romania; 2016.
Sztanó O, Szafián P, Magyar I, Horányi A, Bada G, Hughes DW, Hoyer DL, Wallis RJ. Aggradation and progradation controlled clinothems and deep-water sand delivery model in the Neogene Lake Pannon, Makó Trough, Pannonian Basin, SE Hungary. Glob Planet Change. 2013;103:149–67.
Tóth J, Almási I. Interpretation of observed fluid potential patterns in a deep sedimentary basin under tectonic compression: Hungarian Great Plain, Pannonian Basin. Geofluids. 2001;1(1):11–36.
Trugman DT, Borsa AA, Sandwell DT. Did stresses from the Cerro Prieto Geothermal Field influence the El Mayor-Cucapah rupture sequence? Geophys Res Lett. 2014;41(24):8767–74.
Van Balen R, Cloetingh S. Neural network analyses of stress-induced overpressures in the Pannonian Basin. Geophys J Int. 1995;121(2):532–44.
van der Meer F, Hecker C, van Ruitenbeek F, van der Werff H, de Wijkerslooth C, Wechsler C. Geologic remote sensing for geothermal exploration: a review. Int J Appl Earth Obs Geoinf. 2014;33:255–69.
van Thienen-Visser K, Pruiksma J, Breunese J. Compaction and subsidence of the Groningen gas field in the Netherlands. Proc Int Assoc Hydrol Sci. 2015;372:367–73.
Vasco DW, Karasaki K, Nakagome O. Monitoring production using surface deformation: the Hijiori test site and the Okuaizu geothermal field, Japan. Geothermics. 2002;31(3):303–42.
Vasco D, Rutqvist J, Ferretti A, Rucci A, Bellotti F, Dobson P, Oldenburg C, Garcia J, Walters M, Hartline C. Monitoring deformation at the Geysers Geothermal Field, California using C-band and X-band interferometric synthetic aperture radar. Geophys Res Lett. 2013;40(11):2567–72.
Vass I, Tóth TM, Szanyi J, Kovács B. Hybrid numerical modelling of fluid and heat transport between the overpressured and gravitational flow systems of the Pannonian Basin. Geothermics. 2018;72:268–76.
Yang XM, Davis PM, Dieterich JH. Deformation from inflation of a dipping finite prolate spheroid in an elastic half-space as a model for volcanic stressing. J Geophys Res Solid Earth. 1988;93(B5):4249–57.
Zimmerman RW. Compressibility of sandstones. Amsterdam: Elsevier; 1990.

Publisher's Note